Dynamic Modeling of Chemical Vapor Infiltration

Stratis V. Sotirchos
Dept. of Chemical Engineering, University of Rochester, Rochester, NY 14627

A mathematical model is developed to describe the dynamic and pseudosteady-state behavior of chemical vapor infiltration, a process used to fabricate fiber-reinforced ceramic matrix composites. The three-parameter dusty-gas model is used to describe the interaction of mass transport fluxes, partial pressures, and partial pressure gradients in the interior of the porous medium, with the viscous flux related to the total pressure gradient through Darcy's law. The model is applied to study the deposition of SiC via decomposition of methyltrichlorosilane in a porous medium whose structure can be represented by a population of uniformly-sized, randomly-overlapping pores. The results show that use of simplified mass transport flux models can lead to significantly different results, even if the concentration of reactants is low and the effects of the products of the reaction on the deposition rate are ignored. It is also shown that operation of chemical vapor infiltration reactors under pressure pulsing can lead to conversion gradients in the densifying structure by a few orders of magnitude smaller than those seen at the same reaction conditions under constant pressure.

Introduction

Low-density materials exhibiting noncatastrophic failure are required in many high-temperature aerospace and energy applications. Monolithic ceramics and composites of polymer or metal matrices in general are unsuitable for such applications. Carbon-carbon composites are used in a number of applications, but they have to be protected from oxidation at high temperatures. The requirements of low density and acceptable toughness are satisfied by fiber-reinforced ceramic matrix composites, since fiber reinforcement usually leads to strengthening and toughening of the homogeneous isotropic material that forms the matrix of the composite (Belitskus, 1988). Chemical vapor infiltration (CVI) is the most advantageous of the methods that can be used to fabricate ceramic matrix composites without damaging the preform of fibers or whiskers used for reinforcement. During this process, the gaseous reactants or the products of their decomposition in the gas phase, which surrounds the fibrous preform, are transported through the pores and form a ceramic matrix throughout the preform by chemical vapor deposition. Chemical vapor infiltration leads to products of very good mechanical properties, can produce objects of complex shape and large size, and can be used for many ceramic-ceramic composites including oxides and non-oxides (Stinton et al., 1988; Naslain et al., 1989).

The most serious disadvantage of chemical vapor infiltration lies in its being a slow and, as a result, expensive process. Because of the occurrence of the chemical reaction, the concentration of the gaseous reactants decreases away from the external surface of the preforms and leads to lower deposition rates in the interior. The resistance for mass transport in the preforms increases with decreasing porosity (or equivalently, increasing density), and as a result, the concentration and density gradients become progressively larger. This situation may eventually lead to plugging of the pores at the external surface of the preform, while there is considerable open space left in the interior. Repeated cycles of surface machining to open the surface pores and reaction are thus needed in practice to obtain products of acceptable nonuniformity of density. Middleman et al. (1990) suggested to improve process of isothermal, diffusion-driven chemical vapor infiltration by using nonuniform preforms, with higher (initially) porosity at the external surface, that would eventually evolve toward uniformly densified structures. Such a solution may appear feasible on theoretical grounds; but even if making such preforms is not a practical problem, the improvement would be of limited extent. The initial nonuniformity of the preform should be kept within limits since large nonuniformities in the fiber content of the structure could adversely affect its overall mechanical properties.

To overcome the above problem, researchers at the Oak Ridge National Laboratory developed a forced flow process (ORNL process) (Stinton et al., 1986), which rests in using a pressure gradient to increase the transport rate of the gaseous

reactants in the preform. A temperature gradient is applied against the pressure gradient to compensate for the effects of decreasing concentration on the reaction rate profile. The ORNL process achieves a dramatic reduction in the time needed to obtain densified structures with acceptable density gradients. It, however, requires a specially designed graphite holder to position the sample for application of the pressure gradient, and as a result, it compromises one of the most important advantages of CVI over other methods, namely its flexibility with respect to preform shape and size.

The pressure gradient process enhances the transport rate of the reactants in the preform by exploiting the fact that the resistance for convective mass transport in the porous media encountered in chemical vapor infiltration is lower than that for diffusive transport. Therefore, the same effect can, in principle, be achieved by any process that involves convective mass transport in the porous medium. Some experimental studies, most recently by Sugiyama and coworkers (Sugiyama and Nakamura, 1987; Sugiyama and Yamamoto, 1988), have suggested that the transport rate of the gaseous reactants in the preform can be increased by periodic pressurization and depressurization of the chemical vapor infiltration reactor (pulse CVI). Pulse CVI can be applied to free standing preforms, and consequently, it preserves all the advantages of the conventional isothermal, diffusion-driven process.

Mathematical models of the densification of porous substrates by chemical vapor infiltration help us understand the details of the interaction between the chemical reactions and the various mass transport mechanisms involved in the process. Provided that fundamental information on the kinetics of the reactions and on the evolution of the transport and structural properties of the porous medium with the porosity is available, the mathematical model can be used to identify the operating conditions at which a densified structure of acceptable density gradients can be obtained in the least possible time. All theoretical studies presented thus far have focused on the investigation of the pseudosteady-state or quasi-transient (long-time) behavior of the process (Fitzer and Gadow, 1986; Rossignol et al., 1984; Starr, 1988; Gupte and Tsamopoulos, 1989; Tai and Chou, 1989; Chung et al., 1989; Middleman et al., 1989). Simple diffusion flux models (of the Fick's law type) have been used in most cases to decouple the transport and reaction equations for a 'key' gaseous reactant from those of other species present in the reactor. As a result, the effects of the pressure buildup in the preform and of the interaction of the fluxes of reactants and products have not been investigated. Moreover, the evolution of the structure of the porous preform in the course of the densification process has usually been described by simplistic structural models, much simpler than those presented in the literature for the equivalent, with regard to microstructure evolution, problem of gas-solid reactions with solid product (Sotirchos and Yu, 1985, 1988; Zarkanitis et al., 1990).

A mathematical model is developed in this study to describe the processes of reaction and multicomponent mass transport that take place during chemical vapor deposition of ceramic material in a porous medium under transient conditions. The model is used to study the deposition of silicon carbide within a slab-shaped preform from methyltrichlosilane in the presence of hydrogen. Both the pseudosteady-state (long-time) and short-time dynamic behavior of the system are investigated. The study of the pseudosteady-state behavior of the process focuses on the effects of the complexity of the flux model and of the interaction of the fluxes of the reactants and products on the predictions of the mathematical model. The analysis of the short-time dynamic behavior of the system, on the other hand, concentrates on the effects of pressure pulsing on the average reaction rate profile in the preform: that is, it addresses the question of whether pulse CVI is a feasible approach for reducing the density gradients in the final product. The developed transport and reaction model can be used with any model describing structure evolution during densification. To simplify the analysis of the simulation results, however, a simple structure of uniformly sized pores is employed to obtain the results reported here.

Dynamic Transport and Reaction Model

The transport and reaction model is formulated for the general case, in which n gaseous species participate in m chemical reactions. Some of these reactions are heterogeneous and lead to the formation of a solid product S, which is deposited within the porous structure at the gas-solid interface. Small concentrations of gaseous reactants and low reaction rates are employed in typical applications of CVI, and consequently, the amount of heat released or absorbed by the chemical reactions cannot lead to significant temperature gradients in the densifying structure. Therefore, consideration of the energy balance is not necessary for the description of the system. However, the development of the mathematical model will allow for the existence of temperature gradients to cover the case in which a nonuniform temperature field is externally imposed on the system, like in the application of the ORNL process.

The mass balances (continuity equations) of the gaseous species, expressed in terms of the partial pressures p_i, are written:

$$\frac{\partial(\epsilon^e p_i/RT)}{\partial t} + \nabla \cdot \underline{N}_i = \sum_{\rho} \nu_{i\rho} R_{v\rho} \tag{1}$$

where ϵ^e is the accessible porosity of the porous medium; $\underline{N}_i$ is the molar flux of species i; R is the ideal gas constant; T is the temperature; and $\nu_{i\rho}$ is the stoichiometric coefficient of species i in reaction ρ. $R_{v\rho}$, the volumetric reaction rate (per unit volume of porous medium) of reaction ρ, is given by either of the equations:

$$R_{v\rho} = \epsilon^e R_\rho \quad \text{or} \quad R_{v\rho} = S^e R_{s\rho} \tag{2}$$

where $R_{s\rho}$ is the intrinsic rate of the heterogeneous reaction ρ (per unit area); R_ρ is the rate of the homogeneous reaction ρ (per unit volume of gas phase); and S^e is the accessible internal surface area (per unit volume of porous medium).

The mass balance of the deposited solid expressed in terms of the conversion ξ has the form:

$$\frac{\partial \xi}{\partial t} = \frac{v_S}{\epsilon_0} \sum_{\rho} \nu_{S\rho} R_{v\rho} \tag{3}$$

where v_S is the molar volume of the deposited solid; ϵ_0 is the initial porosity of the preform; and $\nu_{S\rho}$ is the stoichiometric

coefficient of the solid in reaction ρ. Obviously, $\nu_{S\rho}$ is zero for the homogeneous reactions. The conversion used in Eq. 3 is defined as:

$$\xi = \frac{\epsilon_0 - \epsilon}{\epsilon_0} \tag{4}$$

with ϵ being the total porosity of the structure.

The dusty-gas model equations (Mason et al., 1967; Mason and Malinauskas, 1983) are used to describe the coupling of fluxes, partial pressures, and partial pressure gradients in the porous medium. This model is strictly valid for homoporous media only (that is, with uniformly sized pores), but it was recently shown (Sotirchos, 1989) that it provides an excellent approximation for diffusion in heteroporous media as well. According to this model, the fluxes are assumed to consist of additive viscous and diffusive contributions:

$$\underline{N}_i = \underline{N}_i^D + \underline{N}_i^V \tag{5}$$

For negligible thermal diffusion, surface diffusion, and thermal transpiration effects, the diffusive fluxes (superscript D) are related by the equations

$$-\frac{1}{RT}\nabla p_i = \sum_{j \neq i} \frac{x_j \underline{N}_i^D - x_i \underline{N}_j^D}{\mathfrak{D}_{ij}^e} + \frac{\underline{N}_i^D}{D_{Ki}^e} \tag{6}$$

where x_i is the mole fraction of species i, and p is the total pressure. $\mathfrak{D}_{ij}^e$, the effective binary diffusivity for gases i and j, and D_{Ki}^e, the effective Knudsen diffusion coefficient of gas i, are determined using the equations:

$$\mathfrak{D}_{ij}^e = \mathfrak{D}_{ij}^* \left(\frac{p^*}{p}\right)\left(\frac{T}{T^*}\right)^{3/2} S_1; \quad D_{Ki}^e = D_{Ki}^* \left(\frac{T}{T^*}\right)^{1/2} S_2 \tag{7a, b}$$

where $\mathfrak{D}_{ij}^*$ is the binary diffusion coefficient for the (i, j) pair computed at reference pressure and temperature p^* and T^*, and D_{Ki}^* is the Knudsen diffusivity of species i in a capillary of reference radius r^* at reference temperature T^*. Parameters S_1 and S_2 are determined by the structure of the porous medium. Using Eqs. 7a and 7b and rearranging, Eq. 6 becomes:

$$-\frac{1}{R(TT^*)^{1/2}} S_1 \nabla p_i = \sum_{j \neq i} \frac{p_j \underline{N}_i^D - p_i \underline{N}_j^D}{\mathfrak{D}_{ij}^* p^*} + \frac{\underline{N}_i^D}{D_{Ki}^*} \frac{S_1 T}{S_2 T^*} \tag{8}$$

or in matrix form

$$-\frac{S_1}{R(TT^*)^{1/2}} \nabla \boldsymbol{p} = \boldsymbol{B}\underline{N}^D \tag{9}$$

where $\boldsymbol{p}$ is the n-dimensional vector of partial pressures; $\underline{N}^D$ is the n-dimensional vector of diffusive fluxes; and the elements of matrix $\boldsymbol{B}$ are given by:

$$B_{ij} = \frac{-p_i}{\mathfrak{D}_{ij}^* p^*}, \quad j \neq i \tag{10a}$$

$$B_{ii} = \sum_{j \neq i} \frac{p_j}{\mathfrak{D}_{ij}^* p^*} + \frac{1}{D_{Ki}^*} \frac{S_1}{S_2} \frac{T}{T^*} \tag{10b}$$

Darcy's law is used to relate the viscous fluxes (superscript V) to the total pressure gradient:

$$\underline{N}_i^V = -\frac{B^e p_i}{\mu RT} \nabla p \tag{11}$$

B^e is the effective permeability of the porous medium, and μ is the viscosity of the gaseous mixture. It should be noted that Darcy's law is a steady-state result, and consequently it may not be valid when the short-time behavior of the system is considered. The time constant associated with transient effects in the flow of a fluid in a tube of radius r is of the order of r^2/ν (Whitaker, 1967), where ν is the kinematic viscosity of the fluid. For pores with radius in the range 1-50 μm, this gives time constants much smaller than the time scales we are concerned with in this study, even of the case of pressure pulsing.

Equations for the variation of ϵ^e, S^e, S_1, S_2, and B^e with the conversion, as well as a set of appropriate boundary conditions, are needed to complete the mathematical model. These equations may be determined by experiment or by theoretical methods once a physical model for the pore structure of the system is adopted. The latter approach is adopted in the following section.

Application to the SiC/SiC System

The developed mathematical model will be used to study the case where SiC is the matrix material of the composite and methyltrichlorosilane (MTS) decomposition is used for its deposition. Because of their diverse applications, SiC composites have been the most extensively studied system in the area of chemical vapor infiltration. Deposition of SiC from MTS—deposition from dimethyldichlorosilane (DDS) is another of many alternatives—has been used in experimental studies on the ORNL (pressure gradient-thermal gradient) process and is the most frequently used route for SiC deposition, probably because of the observation that carbon formation is kinetically inhibited at moderate temperatures for reactant systems with Si:C ratios near unity (Van Kemenade and Stemfoort, 1972).

Preform geometry and boundary and initial conditions

A slab-shaped preform of thickness $2a$ exposed to a stream of hydrogen and methyltrichlorosilane is considered. The composition of the mixture in the gas phase surrounding the preform is assumed to be the same in both sides, and the standard no-flux (symmetry) boundary conditions are applied at the symmetry plane of the slab. The other set of boundary conditions is obtained by assuming that negligible mass transport limitations exist between the gas phase and the external surface of the preform, that is, by setting the partial pressures of the gaseous species at the external surface of the preform equal to those in the bulk of the gas phase. The boundary conditions thus have the following form.

At $z = 0$:

$$N_i = 0, \quad i = 1, \ldots n \tag{12a}$$

At $z = a$:

$$p_i = p_{ib}, \quad i = 1, \ldots n \tag{12b}$$

p_{ib} is the partial pressure of species i in the bulk of the gas phase.

At time zero, the conversion (or equivalently, porosity) and the partial pressure profiles of the gaseous species are known.

At $t=0$:

$$\xi = \xi_0(z); \quad p_i = p_{i0}(z) \tag{13a, b}$$

This form of initial conditions allows for the case in which the operating conditions (mixture composition and pressure in the reaction chamber) are changed during the process. At the onset of infiltration, the porosity is uniform and equal to the initial porosity of the preform, ϵ_0, the partial pressures of the reactant MTS and product HCl are zero, and the partial pressure of hydrogen is uniform and equal to the pressure of the reactor.

Reactions and kinetics

MTS is assumed to decompose according to the reaction:

$$CH_3Cl_3Si \xrightarrow{H_2} SiC + 3HCl \tag{14}$$

The mechanism of the reaction is undoubtedly more complex than what this equation implies, but in the present study only the above overall reaction will be considered. On the basis of experimental results reported by Brennfleck et al. (1984), the rate expression for the reaction is assumed to have the form:

$$R_s = k_{s0}\exp(-E/RT)p_{\mathrm{MTS}} \tag{15}$$

with

$$k_{s0} = 2.290 \cdot 10^{-2}\ \mathrm{kmol/m^2 \cdot s \cdot atm}; \quad E = 120 \cdot 10^6\ \mathrm{J/kmol}$$

It was shown by Middleman (1989) and Sheldon (1990) that the form of the reaction rate profile in the interior of the preform under diffusion-driven infiltration depends strongly on the kinetic model. However, although the deposition SiC from methyltrichlorosilane (MTS) is among the most extensively studied deposition reactions (Schlichting, 1980; Langlais et al., 1990), there is considerable disagreement in the literature on the mechanism of the reaction, 'overall' activation energy, rate constant, and dependence of the reaction rate on the concentration of MTS. For instance, while first-order dependence has been reported in a number of studies (e.g., Brennfleck et al., 1984), a recent study by Besmann and Johnson (1988) found no dependence of the reaction rate on the concentration of MTS. Moreover, recent studies by Besmann et al. (1991) and Papasouliotis and Sotirchos (1991) showed that the rate of deposition is strongly influenced by the concentration of HCl.

Pore structure evolution

To simplify the analysis of the simulation results, the structure of the preform is represented by a network of uniformly sized cylindrical capillaries of radius r_0. As material starts depositing within the structure of the preform, the radius of pores decreases. It can be shown (Gavalas, 1980; Sotirchos, 1987) that the radius of pores at times different from zero, r, is related to the conversion, or equivalently (see Eq. 4), to the porosity, by the relation:

$$\frac{r}{r_0} = \left[\frac{\ln(1-\epsilon)}{\ln(1-\epsilon_0)}\right]^{1/2} \tag{16}$$

with ϵ_0 being the initial porosity of the structure. A structure of randomly overlapping capillaries does not present formation of inaccessible pore space, and consequently, the accessible values of porosity and surface area, ϵ^e and S^e are equal to the total. Moreover, we have that

$$S_1 = \frac{\epsilon}{3}; \quad S_2 = \frac{\epsilon}{3}\frac{r}{r^*}; \quad B^e = \frac{\epsilon}{3}\frac{r^2}{8}; \quad S = -\frac{2\ln(1-\epsilon)(1-\epsilon)}{r} \tag{17a-d}$$

Computational Aspects

B-spline collocation (De Boor, 1978) is used to discretize the model equations in space, and the resulting set of algebraic and ordinary differential equations is integrated in time using a Gear-type solver (Gear, 1971). Piecewise continuous polynomial interpolation based on cubic splines is used to approximate the partial pressure and conversion profiles over the $[0, a]$ interval. The transport and reaction model is then discretized in space by requiring that the mass balance equations for the gaseous species (Eqs. 1) be satisfied at a number of interior collocation points, two for each subinterval, the boundary conditions (Eqs. 12a and 12b) be satisfied at the end points, and the solid mass balance equation (Eq. 3) be valid both at the interior collocation points and at the end points. For N subintervals, this discretization process leads to $(n+1)2N+2$ ordinary differential equations and $2n$ algebraic equations, the latter resulting from the boundary conditions. If the same discretization scheme is applied to the dusty-gas model equations, that is, piecewise continuous polynomial approximation is also used for the fluxes, $n(2N+2)$ more algebraic equations are obtained, and consequently, the total size of the system that has to be used in the differential-algebraic equation solver is $(2n+1)(2N+2)$.

However, the divergences of the fluxes, $\nabla \cdot \underline{N}_i$, appearing in the mass balance equations, can be computed at every spatial and temporal position using the differentiated form of the dusty-gas model equations. In this way, only the ordinary differential equations that result from the discretization of the mass balance equations and the algebraic equations obtained from the boundary condition must be used in the integrator. This leads to considerable reduction of the computational effort involved in the integration of the discretized system, since the number of algebraic and ordinary differential equations is cut almost in half, from $(2n+1)(2N+2)$ to $(n+1)(2N+2)$. The procedure used to obtain the divergences of the fluxes from the dusty-gas model is described briefly in the following paragraphs. Although for the particular preform geometry that I consider here the problem is one-dimensional, I will retain the vector notation since the procedure can be used in more than one dimension.

Differentiation of Eq. 5 gives:

$$\nabla \cdot \underline{N}_i = \nabla \cdot \underline{N}_i^D + \nabla \cdot \underline{N}_i^V \tag{18}$$

The equation giving the divergence of the viscous contribution

to the flux is obtained by differentiating Eq. 11. We have:

$$\nabla \cdot \underline{N}_i^V = -\frac{B^e (T^*)^{1/2}}{\mu^* R T^{3/2}} (p_i \nabla^2 p + \nabla p_i \cdot \nabla p) - \frac{\nabla B^e (T^*)^{1/2} T^{3/2} - (3/2) B^e (TT^*)^{1/2} \nabla T}{\mu^* R T^3} \cdot p_i \nabla p \quad (19)$$

The equations relating the diffusive fluxes to the partial pressures and their gradients (Eqs. 8 or 9) are implicit in the fluxes, and consequently, it is not possible to obtain analytic expressions for the divergences of the fluxes. Differentiating Eq. 9, we get the set of equations:

$$-\frac{S_1}{R(TT^*)^{1/2}} \nabla^2 \boldsymbol{p} - \frac{\nabla S_1 (TT^*)^{1/2} - (1/2)(T^*/T)^{1/2} S_1 \nabla T}{RTT^*} \cdot \nabla \boldsymbol{p} = \boldsymbol{B} \nabla \cdot \underline{\boldsymbol{N}}^D + (\nabla \boldsymbol{B}) \underline{\boldsymbol{N}}^D \quad (20)$$

with

$$(\nabla B)_{ij} = \frac{-\nabla p_i}{\mathfrak{D}_{ij}^* p^*}, \quad j \neq i \quad (21a)$$

$$(\nabla B)_{ii} = \sum_{j \neq i} \frac{-\nabla p_j}{\mathfrak{D}_{ij}^* p^*} + \frac{1}{D_{Ki}^*} \frac{(\nabla S_1 T + S_1 \nabla T) S_2 - S_1 T \nabla S_2}{T^* S_2^2} \quad (21b)$$

Equation 20 forms a set of linear algebraic equations for the gradients of the fluxes and can thus be solved numerically at every spatial and temporal position. For given T, ∇T, p, ∇p, $\nabla^2 p$, ξ, and $\nabla \xi$, we solve the set of linear algebraic equations (Eq. 9) to compute the diffusive fluxes, $\underline{N}_i^D$. The solution of Eq. 20 for $\nabla \cdot \underline{N}^D$ then follows, and the result is added to that of Eq. 19 (see Eq. 18) to obtain the gradients of the fluxes needed in mass balances. Since the same matrix $\boldsymbol{B}$ appears in Eqs. 9 and 20, the computation of $\nabla \cdot \underline{N}^D$ requires only the computation of the righthand side vector and a back-substitution using the already decomposed, during computation of $\underline{N}^D$ from Eq. 9, form of $\boldsymbol{B}$.

Results and Discussion

Results are discussed here on the dynamic behavior of the chemical vapor deposition of SiC in a slab-shaped, porous preform from methyltrichlorosilane in the presence of hydrogen. The general mathematical model for transient transport and reaction in an evolving porous medium (Eqs. 1–11), supplemented by Eqs. 12–17, was used to obtain the reported results. Since the heat released by the reaction under typical operating conditions is not enough to cause significant temperature gradients in the densifying structure, isothermal operation was considered, with the temperature and pressure of operation set, for most of the results, at 1 atm and 1,300 K, respectively. The Chapman-Enskog equations (Bird et al., 1960) were used to compute the binary diffusion coefficients, and an average value of 3.7×10^{-5} kg/m·s was estimated for the viscosity of the mixture at 1,300 K. The preforms considered in this study have the same initial porosity (50%), but may differ in thickness, $2a$, and average initial pore size, r_0. The parametric sensitivity of the process of chemical vapor infiltration to the structural properties of the preform and to the mode of their evolution with the extent of densification will be the subject of a future study.

Pseudosteady-state behavior

We examine in this section the long-term dynamic behavior of chemical vapor infiltration under constant operating conditions. Since the time constant associated with conversion and structural changes in the preforms is much larger than that for concentration (or equivalently, partial pressure) changes, the long-term dynamic behavior of the system can also be described by a pseudosteady-state (quasi-transient) version of the transport and reaction model, in which only the time derivatives of the conversion and of the structural properties are retained in the model equations. The results reported in this section are thus characterized as pseudosteady state or quasi-transient despite that they have been obtained using the general dynamic model.

Typical results for the evolution of the conversion profile with time are shown in Figure 1 for a preform with 1-mm half-thickness and 1-μm average pore size. The corresponding partial pressure profiles for the gaseous reactant and product (MTS and HCl) are shown in Figure 2. The arrows in Figure 2 indicate the direction of increasing time for the two sets of partial pressure profiles shown there, with the reaction times being the same as those marked on Figure 1. The dimensionless time used to label the curves in the figures has been defined so that complete plugging of the pores of the structure at the ambient conditions would take place at $\tau = 10$, that is,

$$\tau = \frac{10 v_{SiC} k_{s0} \exp(-E/RT_b) (p_{MTS})_b}{r_0} t \quad (22)$$

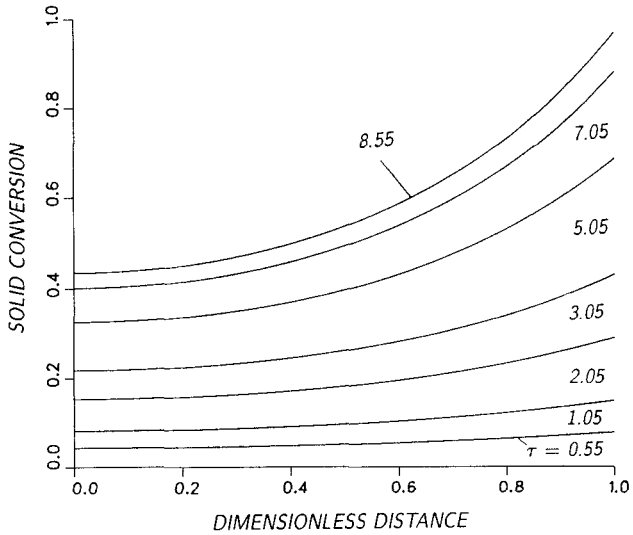

Figure 1. Variation of the solid conversion profile during isothermal densification at constant pressure.

$a = 1$ mm; $x_{MTS} = 0.1$; $x_{H_2} = 0.9$; $r_0 = 1$ μm; $\epsilon_0 = 0.5$; $p_b = 1$ atm; $T_b = 1{,}300$ K; $t = \tau \times 228.9$ s.

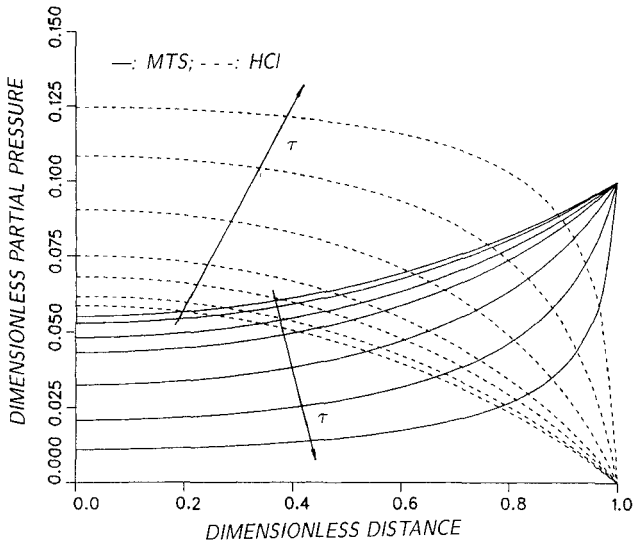

Figure 2. Variation of partial pressure profiles of gases during isothermal densification at constant pressure.

Parameters same as in Figure 1.

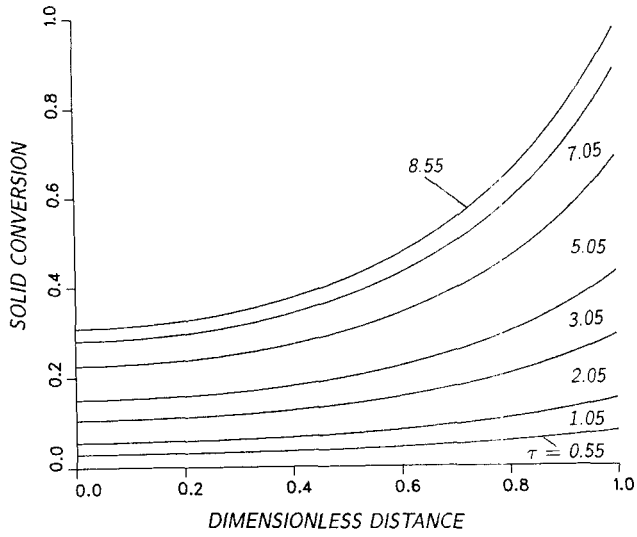

Figure 3. Variation of the solid conversion profile during isothermal densification at constant pressure.

$a = 1$ mm; $x_{MTS} = 0.4$; $x_{H_2} = 0.6$; $r_0 = 1$ μm; $\epsilon_0 = 0.5$; $p_b = 1$ atm; $T = 1{,}300$ K; $t = \tau \times 57.28$ s.

It can be shown using Eqs. 16 and 17d (also see Gavalas, 1980) that the internal surface area increases with decreasing porosity during the initial stages of the reaction, reaching a maximum at $\epsilon = 1 - e^{-1/2} = 0.393$. The surface area increase leads to higher local reaction rates, which in conjunction with the decreasing effective diffusion coefficients, cause steeper concentration and hence conversion profiles in the interior of the preform (see Figures 1 and 2). The surface area starts to decrease for porosities lower than 0.393, but the effect of its decrease on the concentration and conversion gradients is offset by that of the diminishing mass transport coefficients (see Eqs. 17a-17c).

The results of Figures 1 and 2 were obtained for MTS:H_2 ratio equal to 1:9 (mol/mol). Results for a higher reactant:inert ratio (namely, 4:6) are shown in Figures 3 and 4, with all other parameters being the same as in Figures 1 and 2. Comparison of Figures 3 and 4 with Figures 1 and 2, respectively, shows that larger MTS:H_2 ratios cause larger concentration (partial pressure) and density (conversion) gradients in the preforms. For instance, the conversion reached at the center of the preform at $\tau = 8.55$ with 0.4 atm of MTS present in the reactor (Figure 3) is about 30% lower than that reached for 0.1 atm of MTS (Figure 1). An analogous observation holds for the reduced partial pressure of MTS ($p_{MTS}/p_{MTS,b}$) at the center of the preform, especially during the initial stages of the process. (Note that the actual time corresponding to a certain value of dimensionless time is four times greater in Figures 1 and 2 than in Figures 3 and 4, because of the four times greater partial pressure of MTS in the latter, Eq. 22.) These differences underscore the importance of using the complete form of the dusty-gas model equations in the modeling of the process. If Fick's law without convection is used to relate the flux of MTS to its partial pressure gradient, the profiles of conversion and reduced partial pressure of MTS are independent of the partial pressure of MTS in the reactor. From a practical point of view, the results of Figures 3 and 4 should be seen only as indicative of the effects of the interaction of fluxes on the conversion and partial pressure gradients. Several experimental studies have reported that MTS:H_2 ratios much larger than 1:10 favor the deposition of excess carbon within the preforms.

The partial pressure of H_2 in the interior of the preform remains almost uniform during the reaction (Figure 4). Using the results of Figure 4 for the partial pressures of the three species, one finds that this is also the case for the total pressure within the densifying structure. Since the reaction increases the number of molecules in the gas phase, a pressure buildup takes place within the preform, but even with 40% MTS present in the reactor (Figure 4), the pressure at the center is only 5% higher. Such a pressure rise cannot explain the observed dif-

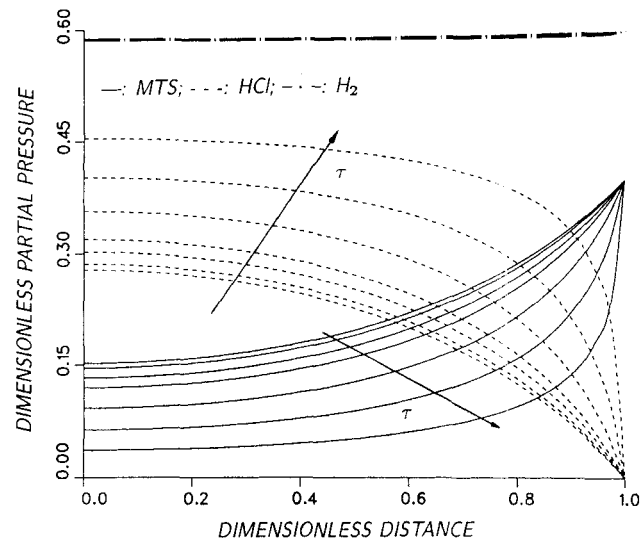

Figure 4. Variation of partial pressure profiles of gases during isothermal densification at constant pressure.

Parameters same as in Figure 3.

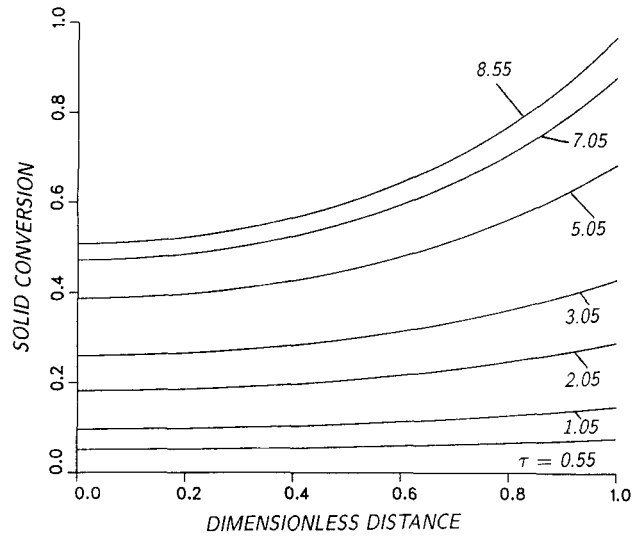

Figure 5. Variation of the solid conversion profile during isothermal densification at constant pressure.

Fick's law for each species without convective terms. $a = 1$ mm; $x_{MTS} = 0.1$; $x_{H_2} = 0.9$; $r_0 = 1$ μm; $\epsilon_0 = 0.5$; $p_b = 1$ atm; $T_b = 1{,}300$ K; $t = \tau \times 228.9$ s.

ferences between the results of Figures 1 and 2 and Figures 3 and 4. The parametric investigation of the problem showed that the pseudosteady-state profile of the partial pressure of MTS changes imperceptibly when the viscous terms are dropped from the dusty-gas model equations and that the main reason behind the rather strong effect of the ambient concentration of MTS on the variation of the quasi-transient conversion and partial pressure profiles with the dimensionless time is the interaction of the diffusion of HCl with that of MTS. The large concentration gradient of HCl (see Figures 2 and 4) causes

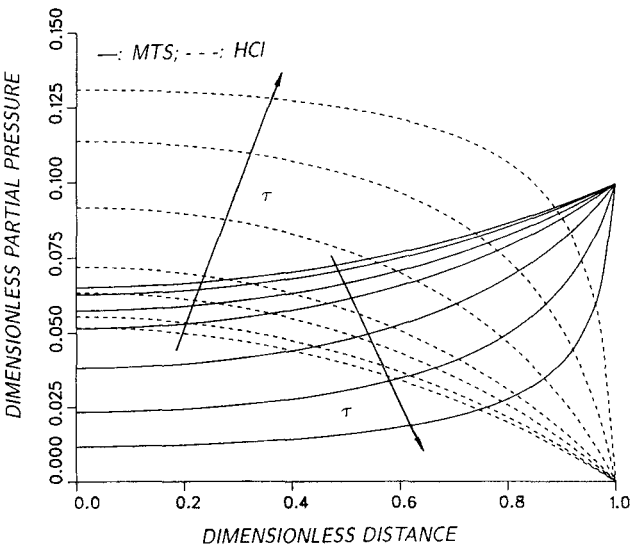

Figure 6. Variation of partial pressure profiles of gases during isothermal densification at constant pressure.

Fick's law for each species without convective terms. Parameters same as in Figure 3.

a large diffusion flux toward the exit of the preform that interferes with the inward movement of the MTS molecules. This interaction is expressed by the cross-diffusion terms in the dusty-gas model equations, that is, the off-diagonal terms in the matrix form of the dusty-gas model.

The effects of the cross-diffusion terms on the behavior of the process may be seen more clearly in Figures 5 and 6, which present the predicted conversion and partial pressure profiles for the densification problem considered in Figures 1 and 2 if we use Fick's law without convective flow in the mathematical model, that is, we write for the fluxes of HCl and MTS:

$$\underline{N}_i = -\frac{D_i^e}{RT}\nabla p_i; \quad \frac{1}{D_i^e} = \frac{1}{D_{Ki}^e} + \frac{1}{\mathfrak{D}_{i,H_2}^e} \tag{23a,b}$$

Comparison of the results of Figures 5 and 6 with those of Figures 1 and 2 shows that simplification of the flux model, namely, omission of the cross-diffusion terms and, secondarily, of the viscous terms, leads to overprediction of the conversion at the center of the preform by almost 20% despite having only 10% MTS present in the reactor. The simplified flux model also overpredicts the partial pressure of HCl in the preform, but this is mainly due to the omission of the viscous terms.

The results of Figures 1 and 2 indicate that to obtain 'uniform' densification of a preform with 1-μm initial pore size, the reaction has to be carried out under milder conditions even for only 1-mm half-thickness. These conditions must either achieve lower reaction rates or increase the transport rate of the reactant in the preform. The reaction rate can, of course, be lowered by decreasing the reaction temperature. This also decreases the mass transport rate, but the transport coefficients exhibit a much weaker dependence on the reaction temperature than the reaction rate constant. Another alternative is to reduce the overall pressure of the reaction, and provided that diffusion occurs in the transition or bulk diffusion regime, to increase the value of the overall effective diffusion coefficient (see Eq. 23b). However, it is not necessary to maintain the temperature and pressure of the reaction constant with the progress of densification. For example, one could vary the temperature or pressure in such a way that the center to surface conversion (or porosity) ratio is maintained close to some acceptable level.

Although the simplified flux model (Fick's law and no viscous terms) overpredicts the conversion in the interior of the preform, the Thiele modulus based on the effective diffusivity defined by Eq. 23b,

$$\Phi^2 = a^2 \frac{RT_b k_{s0} \exp(-E/RT_b) S}{D_{MTS}^e} \tag{24}$$

may be used to determine the reaction temperature and pressure that will keep the center to surface conversion ratio close to a desired value. Figure 7 shows how the temperature and the pressure of the reaction would have to be changed with time to keep the Thiele modulus based on the structural properties at the external surface of the preform equal to 1.0 when $a = 1$ mm and $r_0 = 1$ μm. If the mass transport process could be described by Fick's law without convective flow and the structural properties of the interior preform were the same as those at its surface, the center to surface conversion ratio would be

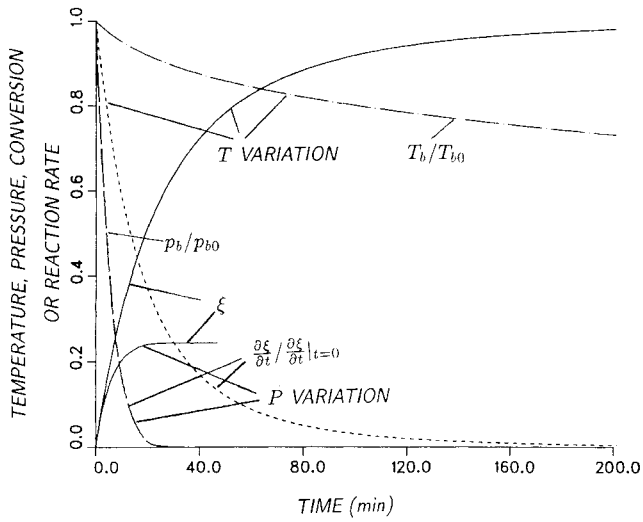

Figure 7. Variation of dimensionless temperature (or pressure), conversion, and reaction rate for constant Thiele modulus (= 1).

$a = 1$ mm; $x_{MTS} = 0.1$; $x_{H_2} = 0.9$; $r_0 = 1$ μm; $\epsilon_0 = 0.5$; $p_{b0} = 1$ atm; $T_{b0} = 1{,}314.6$ K.

equal to $1/\cosh\Phi$, the partial pressure ratio of MTS (0.648 for $\Phi^2 = 1$). Figure 8 presents the same curves as Figure 7 for a preform with larger pores, 20 μm in radius. The half-thickness was chosen as 6.86 mm so that the preform would have the same Thiele modulus *at 1,300 K and 1 atm* as the slab of Figures 1-7 (with $a = 1$ mm and $r_0 = 1$ μm).

According to the results of Figures 7 and 8, the temperature of the reaction must be reduced significantly from its initial value to maintain the Thiele modulus constant and the center to surface conversion ratio close to the desired value at high conversion levels. Because of the exponential dependence of

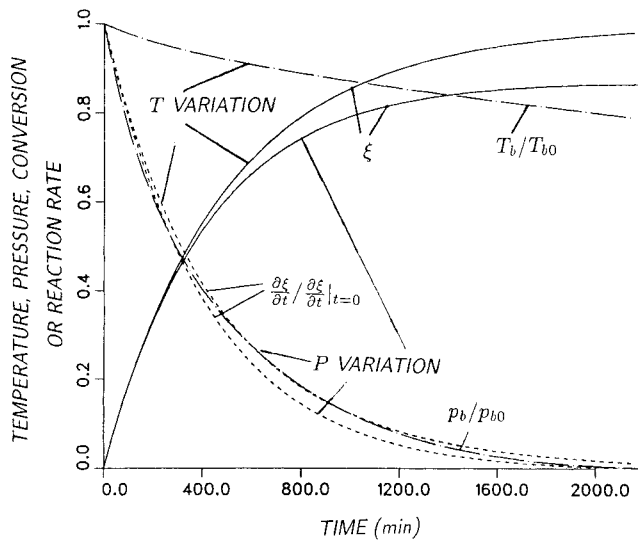

Figure 8. Variation of dimensionless temperature (or pressure), conversion, and reaction rate for constant Thiele modulus (= 1).

$a = 6.86$ mm; $x_{MTS} = 0.1$; $x_{H_2} = 0.9$; $r_0 = 20$ μm; $\epsilon_0 = 0.5$; $p_{b0} = 1$ atm; $T_{b0} = 1{,}315.4$ K.

the reaction rate on temperature, the temperature decrease brings about a dramatic drop in the reaction rate. The diffusion process moves closer to the bulk diffusion regime with increasing pore size, and as a result, the effective diffusion coefficient (Eq. 23b) decreases slower with increasing conversion. For this reason, a smaller change in temperature is needed to keep the Thiele modulus constant for larger initial pore size (compare the T variation curves in Figures 7 and 8).

When the pressure is decreased to maintain the Thiele modulus constant, it is not always possible to cover the whole range of conversion. As the pressure decreases, molecule-molecule collisions become rare, and Knudsen diffusion becomes the dominant mode of mass transport in the porous medium. Thus, beyond some conversion level (or equivalently, pore size), further decrease in pressure has no effect on the value of the effective diffusion coefficient. The maximum attainable conversion level decreases with decreasing initial pore size, reflecting the fact that the diffusion process is closer to the Knudsen diffusion regime for smaller pores. Thus, note that for 1-μm pores the maximum conversion is about 25%, while in the case of 20-μm pores it is possible to cover conversions up to 85%. When both p variation and T variation are feasible, Figures 7 and 8 suggest that smaller reaction times are needed to attain a certain conversion level if T variation is applied. However, several other factors must be taken into account before a certain pattern of pressure or temperature variation is chosen for a CVI system. In most chemical vapor deposition reactions, the composition and structure of the deposited solid are a strong function of the processing conditions, and there is a certain window of operating conditions that produce deposits of acceptable mechanical properties. For instance, for SiC deposition from MTS, reaction temperatures of less than 950°C lead to Si as the primary deposition product.

Infinitely many scenarios of temperature and pressure variation (independently or simultaneously) can be followed to obtain the desired center to surface conversion ratio at the final conversion level. The center to surface conversion ratio, ξ_c/ξ_s, is given for the case considered in this application by the equation:

$$\frac{\xi_c}{\xi_s} = \frac{1}{\xi_s} \int_0^{\xi_s} \frac{(R_v)_c}{(R_v)_s} \, d\xi \tag{25}$$

On the other hand, the time needed to achieve a certain conversion level at the surface of the preform is given by the formula:

$$t = \frac{\epsilon_0}{v_S} \int_0^{\xi_s} \frac{d\xi}{(R_v)_c} \tag{26}$$

Given ξ_s and ξ_c/ξ_s, Eqs. 25 and 26 define an optimization problem, which consists of finding the optimal temperature and or pressure change policies that yield the desired conversion ratio at a certain surface conversion level in the least reaction time.

Dynamic behavior

The short-time dynamic behavior of chemical vapor infiltration during instantaneous pressurization and depressurization is examined in this section. In the first case, the pressure

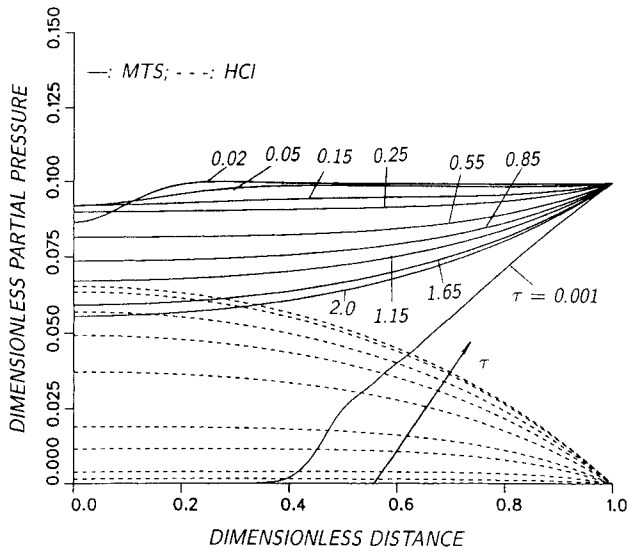

Figure 9. Evolution of partial pressure profiles of MTS and HCl during pressurization.

$a = 6.86$ mm; $x_{MTS} = 0.1$; $x_{H_2} = 0.9$; $r_0 = 20$ μm; $\epsilon_0 = 0.5$; $p_b = 1$ atm; $T_b = 1{,}300$ K; $t = \tau \times 0.107$ s.

in the gas phase that surrounds the porous preform is raised from zero and held at a constant level. During depressurization, on the other hand, the pressure in the reactor is instantaneously reduced and held at zero while the pressure profiles in the interior are at pseudosteady state or some other transient state. The choice of these two modes of pressure change in the reactor was motivated by the importance of these results for understanding the effects of pressure pulsing on the process (pulse CVI) for the particular case in which rectangular wave pulses are employed.

Figure 9 describes the evolution of the partial pressure profiles of MTS and HCl in a preform with 6.86-mm half-thickness and 20-μm initial pore size after instantaneous ($t = 0$) pressurization of the CVI reactor from 0 to 1 atm. As mentioned before, this preform has at 1,000 K and 1 atm the same Thiele modulus as a preform with $a = 1$ mm and $r_0 = 1$ μm; consequently, its initial pseudosteady-state partial pressure profiles are similar to those shown in Figure 2 for low conversions ($\tau = 0.55$). The evolution of the partial pressure profile of H_2 during pressurization is shown in Figure 10. The dimensionless time used to identify the curves of Figures 9 and 10 and of the other figures shown in this section is defined as $\tau = t\mathfrak{D}_{MTS,H_2}/a^2$. The evolution of the partial pressure profiles seen in Figures 9 and 10 indicates that after pressurization of the reaction chamber, the interior of the preform is almost instantaneously filled with the reactive mixture at the ambient composition and pressure. Total pressure equilibration appears to take place in less than 0.02 dimensionless units of time, and then the partial pressure profile of MTS starts to move downward approaching pseudosteady state. HCl also approaches its pseudosteady-state partial pressure profile, but in the opposite direction since there is no HCl present in the reactor initially.

The evolution of the partial pressure profiles of MTS and HCl in the preform of Figure 9 following depressurization of the gas phase, assumed to be instantaneously carried out from 1 to 0 atm at $\tau = 2$, is shown in Figure 11, while the corresponding evolution of the partial pressure profile of the inert gas, H_2, is displayed in Figure 10. According to Figures 10 and 11, the partial pressures of all species in the preform approach steady state (they become almost zero) in a relatively short time interval of the same order of magnitude as the time needed for pressure equilibration in the preform during pressurization but much smaller than the time it takes for the partial pressure profiles of MTS and HCl to relax to pseudosteady state. This is a very important observation for the application of CVI under pressure pulsing conditions. First, it indicates that the duration of the depressurization step for pressure pulsing in a rectangular wave mode does not have to be as large as that of the pressurization step, and consequently, the time during which low reaction rates prevail in the preform would be a small

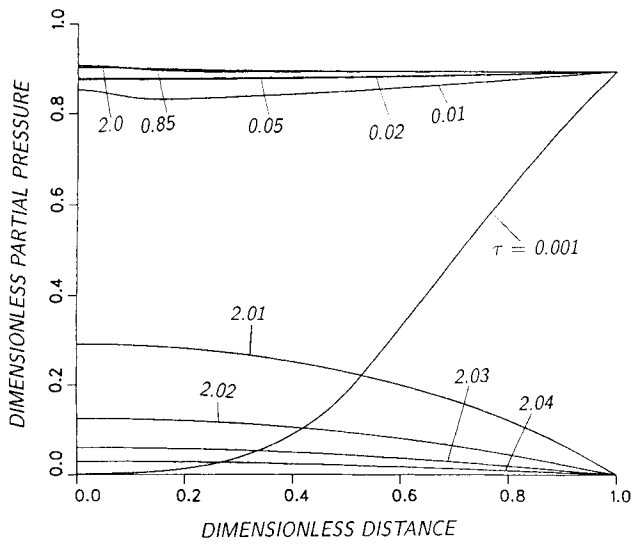

Figure 10. Evolution of the partial pressure profile of H_2 during pressurization and depressurization.

Parameters same as in Figure 9.

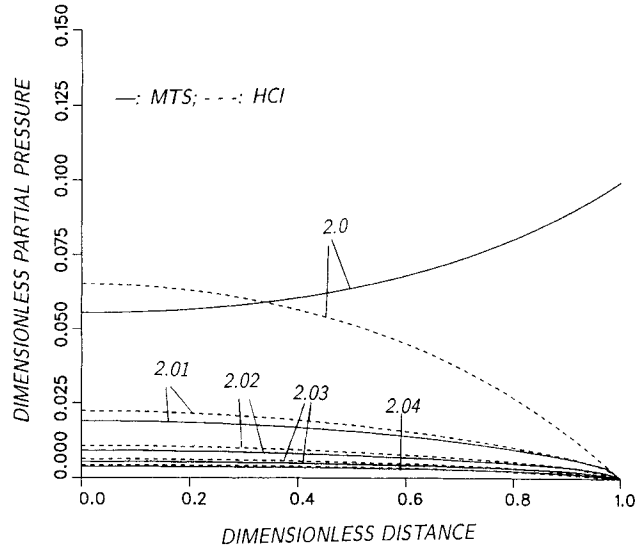

Figure 11. Evolution of partial pressure profiles of MTS and HCl during depressurization.

Parameters same as in Figure 9.

fraction of the total reaction time. Second, it implies that the actual depressurization rate of the preform will chiefly depend on how fast the pressure in the reaction chamber can be reduced.

For the reactive mixture composition, preform thickness, and pore size used in Figures 9–11, the initial (zero conversion) pseudosteady-state partial pressures of MTS and HCl at the center of the preform are 0.0481 and 0.0626 atm, respectively. Since the reaction rate is assumed to be proportional to the partial pressure of MTS in the preform, the initial center to surface conversion ratio, ξ_c/ξ_s, for infiltration under pseudosteady-state conditions should be equal to 0.481. With the exception of the initial stages of the pressurization step ($\tau < 0.02$ in Figure 9), the partial pressure of MTS at every point of the interior of the preform is higher than the corresponding pseudosteady-state value at all times, and thus, the center to surface conversion ratio during pressurization turns out to be larger than the initial pseudosteady-state value; for instance, 0.719 at $\tau = 2$ for the case studied in Figure 9. The partial pressure of HCl, on the other hand, is lower at all times than its pseudosteady-state value. Consequently, if kinetic expressions that account for the possibly decelerating effect of HCl on the reaction rate are employed in the mathematical model, much larger differences between the pulse and pseudosteady-state ξ_c/ξ_s values may be obtained.

Nevertheless, even in the case in which the rate depends on the MTS partial pressure only, a much more dramatic improvement of the uniformity of deposition, covering a few orders of magnitude, may be observed under conditions of strong diffusional limitations. Figure 12 presents the variation of the center to surface conversion ratio for a preform with 10-cm half-thickness and 50-μm initial pore size. (To investigate the effects of internal diffusional limitations without changing more than one of the parameters of the process, it was decided to treat the pre-exponential factor of the rate expression as a model parameter by introducing a dimensionless variable ω, which has the value 1.0 for the kinetic data of Brennfleck et al.) Initially, only the external surface of the preform is exposed to the gaseous reactant, and thus the center to surface conversion ratio is zero. The center to surface conversion ratio starts to increase as the concentration at the center rises, but since the concentration at the interior points decreases after pressure equilibration takes place, it goes through a maximum. The effect of the higher initial concentration becomes progressively weaker as the pressurization time increases, and eventually the conversion profile in the interior of the preform differs insignificantly from the pseudosteady-state profile. For successful application of the pulse-CVI method, one should obviously depressurize the reactor while the partial pressure of the reactant is far from pseudosteady state.

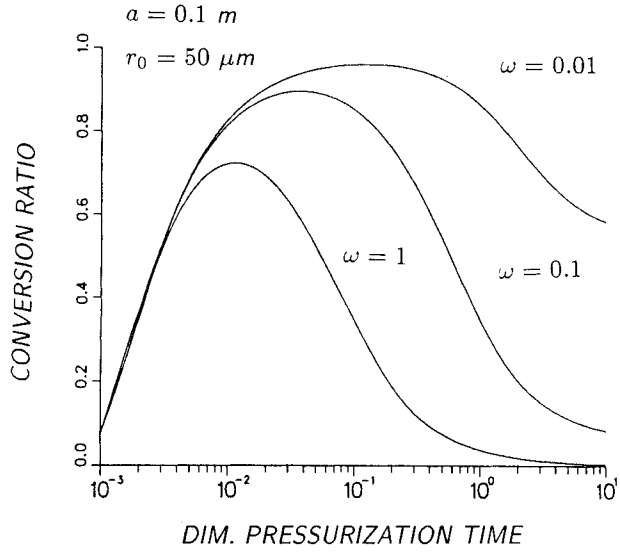

Figure 12. Conversion ratio (center/surface) vs. pressurization time for different reaction rate constants.

$x_{MTS} = 0.1$; $x_{H_2} = 0.9$; $p_b = 1$ atm; $T_b = 1{,}300$ K; $t = \tau \times 22.74$ s.

The center to surface conversion ratio at the maximum for the cases shown in Figure 12 is considerably larger than that prevailing under pseudosteady-state conditions:

ω	$(\xi_c/\xi_s)_{max}$	$(\xi_c/\xi_s)_{steady\text{-}state}$
1	0.722	4.5×10^{-5}
0.1	0.894	5.5×10^{-2}
0.01	0.960	0.53

The relative difference between the pseudosteady-state and maximum value (Figure 12) of the center to surface conversion ratio increases with increasing reaction rate constant, while the maximum itself, as well as the time at which it occurs, becomes smaller. For $\omega = 1$ the maximum ξ_c/ξ_s under pressure pulsing is larger than the initial pseudosteady-state ratio by more than four orders of magnitude, while for $\omega = 0.01$ the two values differ only by a factor of 1.8. Even in the latter case, however, the improvement is more than significant since to obtain the maximum center to surface conversion ratio under pseudosteady-state conditions (see the previous section), the reaction rate must be slowed down by a factor of about 18.85 (estimated for the simple flux model of Eq. 23). The maximum ratio and the time at which it occurs decrease with increasing reaction rate constant, because the reactant partial pressure approaches faster its pseudosteady-state profile and consequently the interior of the preform experiences concentrations larger than the pseudosteady state for a smaller period of time. The time at which the maximum occurs turns out to be roughly inversely proportional to the square root of the reaction rate constant. The center to surface conversion ratio improves further during depressurization since the partial pressure of the reactant decreases from the center to the surface (see Figure 11). However, since depressurization is a very fast process, this improvement is practically insignificant.

The evolution of partial pressure profiles during pressurization points to the conclusion that unsteady operation of the chemical vapor infiltration reactor under pressure pulsing decreases the density gradients in the preform mainly by enhancing the transport rate of the gaseous reactant in the porous structure. Like the pressure gradient process (ORNL process), operation under pressure pulsing exploits the fact that the resistance for convective mass transport in a porous medium with relatively large pores is significantly smaller than that for purely diffusive transport. Both pressure equilibration takes place, the supply rate of chemical reactant to the interior of the preform is much larger than the consumption rate by chem-

ical reaction; as a result, it is possible for the interior of the preform to be filled with reactant at the ambient concentration. Once pressure equilibration takes place, diffusion becomes the primary mode of mass transport—actually convection counteracts the inward movement of the reactant since the pressure decreases from the center to the surface—and the partial pressure of MTS in the interior of the preform starts to decrease approaching steady state.

The total molar flux of species i in a multicomponent mixture can be written as $\underline{N}_i = \underline{J}_i + x_i \underline{N}$, where $\underline{J}_i$ is the flux of species i relative to the molar-average velocity of the fluid mixture and $\underline{N}$ is the total molar bulk flow flux of the mixture (Bird et al., 1960). In the context of the present study, $\underline{J}_i$ is considered to be the contribution of purely diffusive transport to the total flux of gas i, while $x_i \underline{N}$ is the flux of convective mass transport. For a multicomponent mixture consisting of species of identical properties, one can show using the dusty-gas model:

$$\underline{N} = \left(D_K^e + \frac{B^e p}{\mu}\right)\frac{1}{RT}\nabla p; \quad \underline{J}_i = \left(\frac{1}{D_K^e} + \frac{1}{\mathfrak{D}^e}\right)^{-1}\frac{p}{RT}\nabla x_i \quad (27a,b)$$

where $\mathfrak{D}^e$ and D_K^e are the common effective binary and Knudsen diffusion coefficients. In the general case of a multicomponent mixture of dissimilar species, the total convective flux $\underline{N}$ is not zero under isobaric conditions, but it is still possible to write equations similar to Eqs. 27a and 27b in terms of n auxiliary species (pseudospecies), whose fluxes and mole fraction gradients are linear combinations of the fluxes and partial pressure gradients, respectively, of the actual species (Sotirchos, 1989). Equations 27a and 27b imply that the convective flow may be viewed as consisting of additive contributions of viscous and Knudsen flow, while the overall resistance for diffusive transport can be expressed as a series combination of the resistances for Knudsen and binary diffusion. For geometrically similar porous structures of the same porosity, the resistance for viscous transport is inversely proportional to the square of a length scale characteristic of the average pore size, the Knudsen diffusivity is proportional to this length scale, and the effective binary diffusion coefficient is independent of it (see Eqs. 17a and 17b). Therefore, as the average pore size decreases, the resistances for the two modes of mass transport may become comparable to each other, in which case it will be impossible to enhance the transport rate in the preform by pressure pulsing or operation under a pressure gradient.

This situation is demonstrated in Figures 13 and 14, which present the evolution of the MTS and HCl partial pressure profiles during pressurization and depressurization, respectively, in a preform of the same size as that of Figures 9 and 11, but with 1-μm initial pore size. (Note that for the comparison of Figures 13 and 14 to Figures 9 and 11, we have kept the initial Thiele modulus the same by decreasing the preexponential factor of the reaction for the smaller pore size.) Because of the higher resistance for mass transport, the partial pressure profiles during pressurization evolve much more slowly in Figure 13 than in Figure 9. The MTS partial pressure in the interior of the preform of Figure 13 never exceeds the pseudosteady-state value, and therefore pressure pulsing will lead to higher density gradients for this case during pressurization no matter what value of pulsing time is used. Depressurization is also slow (see Figure 14), requiring more than two units of time for the partial pressure in the interior to reach levels

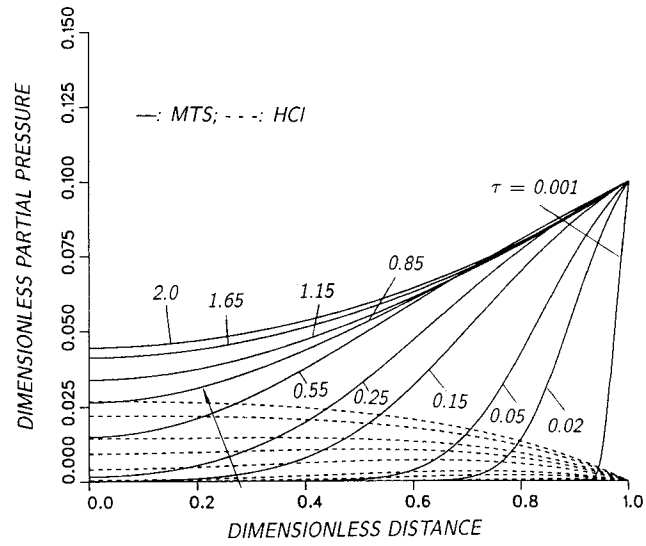

Figure 13. Evolution of partial pressure profiles of MTS and HCl during pressurization.

$a = 6.86$ mm; $x_{MTS} = 0.1$; $x_{H_2} = 0.9$; $r_0 = 1$ μm; $\epsilon_0 = 0.5$; $p_b = 1$ atm; $T_b = 1{,}300$ K; $\omega = 0.02404$; $t = \tau \times 0.107$ s.

attained in less than 0.02 units of dimensionless time in the preform with 20 μm of pore size. Since depressurization lasts longer, its effect on the density gradients in the preform is not insignificant as in the case of the preform of Figures 9-11. The center to surface conversion ratio improves from 0.259 at the end of pressurization to 0.436 at $\tau = 3.35$, but it is still lower than the initial pseudosteady-state ratio of 0.540.

The effects of average pore size on the behavior of CVI under pressure pulsing may be better understood by examining how the mass transport coefficients for viscous flow, Knudsen diffusion (or flow), and binary diffusion vary with the pore size in a preform with 50% porosity. Figure 15 shows this as well as the variation in the effective diffusion coefficient of MTS given by Eq. 23b. We see that at total pressure of 1 atm—

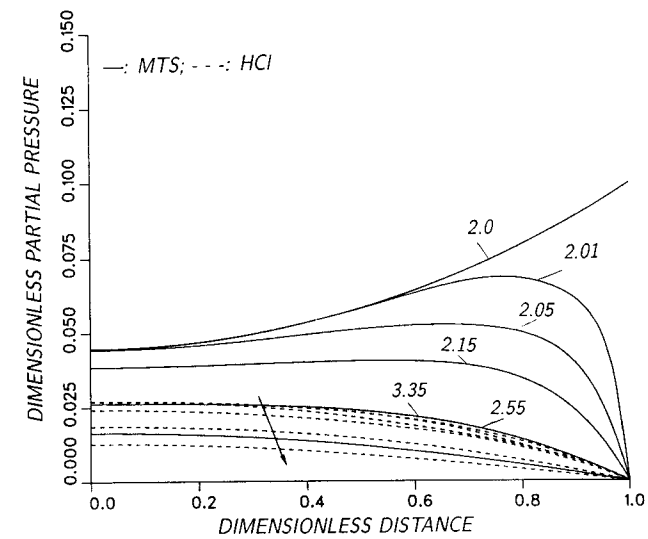

Figure 14. Evolution of partial pressure profiles of MTS and HCl during depressurization.

Parameters same as in Figure 13.

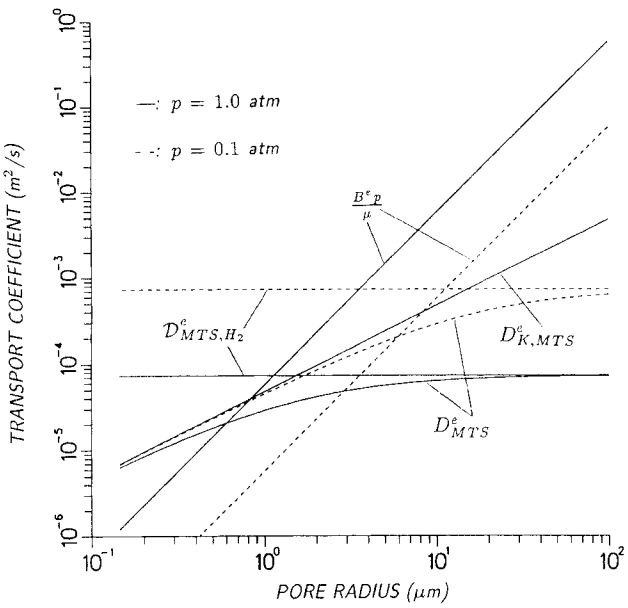

Figure 15. Mass transport coefficients vs. pore radius at 1,300 K.

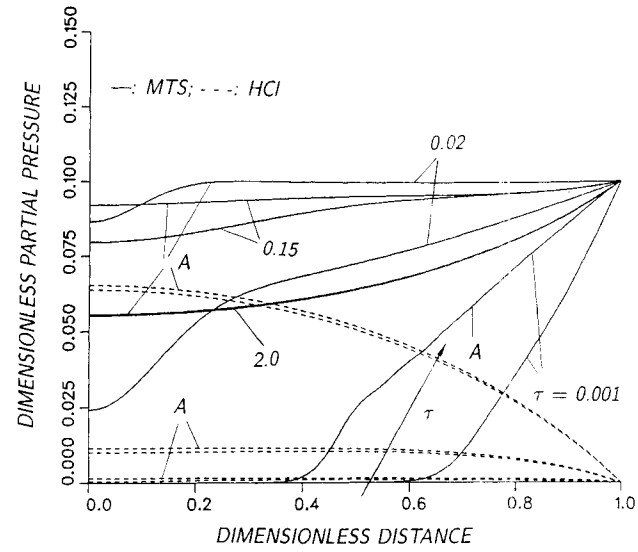

Figure 16. Effects of viscous terms on the evolution of partial pressure profiles of MTS and HCl during pressurization.

A, with viscous terms; *B*, without viscous terms. Parameters same as in Figure 9.

the maximum pressure used in Figures 9–14—the coefficients for the various mechanisms of mass transport become comparable in the neighborhood of 1 μm. Consequently, one would expect to be possible to use convection to enhance the rate of mass transport in the preform only for average pore sizes much larger than this value, in agreement with the results of Figures 9 and 13. The coefficient for viscous transport $B^e p/\mu$ depends linearly on the total pressure, while the binary diffusion coefficient is inversely proportional to it. Therefore, the pore size at which the two coefficients become the same is inversely proportional to the pressure. It could thus be argued that the minimum pore size above which pulsing is a viable option for increasing the deposition uniformity in the preform will increase as the upper limit of the range of pressure variation during pulsing decreases.

We have seen (Eq. 27a) that the convective current arising in a porous medium in the presence of pressure gradients is due to not only viscous flow but also Knudsen flow. Therefore, provided that the resistance for Knudsen flow (diffusion) is larger than that for binary diffusion, it is possible to predict reduction of the density gradients (increase of the center to surface conversion ratio) by pressure pulsing, relative to those obtained under pseudosteady-state conditions, even if the viscous flow terms are not included in the dusty-gas model. Results for the case without viscous terms in the dusty-gas model were presented in a preliminary study of the dynamics of chemical vapor infiltration (Sotirchos and Tomadakis, 1990), where the potential of pressure pulsing for reducing the time needed to obtain preforms with acceptable gradients was demonstrated for the first time. The effects of the viscous terms may be seen in Figure 16, where the MTS and HCl profiles of Figure 9 are compared at selected time instants with those predicted by the mathematical model if the viscous terms are not included in the dusty-gas model. Observe that the preform is still filled with the reactive mixture at concentrations higher than the pseudosteady state. However, since viscous flow works in parallel with Knudsen flow in the presence of pressure gradients, lower MTS partial pressures are reached in the interior before pressure equilibration takes place, and the center to surface conversion ratio is underpredicted if the viscous flow terms are neglected.

Conclusions

A mathematical model was developed to describe the transient transport and reaction phenomena occurring in a multicomponent mixture of reactive and inert gases during chemical vapor infiltration, that is, densification of a porous substrate by chemical vapor deposition of ceramic material. The three-parameter dusty-gas model was used to describe the coupling of mass transport fluxes, partial pressures, and partial pressure gradients in the porous medium, and Darcy's law was employed to relate the viscous flux to the total pressure gradient. Although isothermal operation was assumed in the application considered in this study, the multicomponent transport and reaction model was formulated for the general situation of having a nonuniform temperature field imposed externally on the porous preform.

The developed mathematical model was used to study the transient behavior of the deposition of SiC through decomposition of methyltrichlorosilane in the presence of hydrogen in a slab-shaped preform, whose pore structure can be locally represented by a population of randomly overlapping pores of uniform size. The mathematical model equations were solved using a combination of spatial discretization by collocation on finite elements (*B*-splines) and temporal integration of the resulting set of ordinary differential and algebraic equations. Considerable reduction in the computational time needed for the numerical solution of the model equations was achieved by using the differentiated form of the dusty-gas model equations to compute the divergences of the mass transport fluxes appearing in the continuity equations (mass balances) of the gaseous species. We investigated both the long-time transient

behavior of the process under constant operating conditions (pseudosteady-state behavior) and the short-time evolution of the partial pressure and conversion (density) profiles in the preform during instantaneous pressurization or depressurization of the reaction chamber. The latter results were used to assess the feasibility of operation under pressure pulsing for reducing the density gradients in the densifying structures.

Our results showed that for accurate predictions of the partial pressure, reaction rate, and conversion profiles in the preforms, it is essential that the complete form of the dusty-gas model equations be used to describe the mass transport process in the porous medium. Even when the mole fraction of reactant in the reactor is small and the reaction rate is independent of the concentrations of the reaction products, simplified flux models (for example, Fick's law without convective flow for each species) tend to overestimate the concentration of the reactant in the interior of the solid and overpredict the rate of reaction. This is due mainly to the omission of the cross-diffusion terms that account for the interference of the outward movement of the products of the reaction with the inward transport of the molecules of the gaseous reactant. As densification proceeds, the consumption rate of the reactant decreases slower than the mass transport rate in the preform; as a result, steeper partial pressure and conversion (density) gradients develop in the preform. It was shown that this problem can be avoided by judicious variation (reduction) of the temperature and (or) pressure of the reaction in the course of the densification process, and a procedure that may be used to identify optimal pressure and (or) temperature reduction histories was suggested.

The results obtained on the short-time behavior of chemical vapor infiltration during sudden pressurization or depressurization revealed that operation under pressure pulsing can lead to smaller density gradients in the densifying porous medium, by a few orders of magnitude in some cases, than those seen under constant pressure at the same conditions. Higher average reaction rates can, therefore, be used during densification under pressure pulsing, and a dramatic reduction of the reaction time needed to obtain ceramic matrix composites of acceptable density gradients may be achieved. Such an improvement is possible only if the resistance for convective transport in the preform is significantly lower than that for diffusive transport, since pressure pulsing (or in general, operation under a pressure gradient) uses convection to enhance the transport rate of gaseous reactants in the porous medium. The resistance for convective transport increases faster with decreasing pore size, and thus, there is a minimum pore size below which pressure pulsing or operation under a pressure gradient is not a viable option for reducing the density gradients in the preform in a given pressure range. The minimum pore size at which the two resistances become comparable moves toward lower values with increasing pressure. Since the average pore opening in a densifying structure decreases with increasing conversion, the optimal conditions for pressure pulsing (range of pressure variation and pulsing time for instance) are expected to change with the progress of densification.

Notation

a = half-thickness of the preform, m
$\boldsymbol{B}$ = matrix defined in Eqs. 9 and 10
B^e = effective permeability of the porous medium, m^2
D_i^e = effective diffusion coefficient of species i (see Eq. 23b), m^2/s
$\mathcal{D}_{ij}$, $\mathcal{D}_{ij}^e$ = binary diffusivity of the (i, j) pair and effective binary diffusivity, respectively, m^2/s
D_{Ki}, D_{Ki}^e = Knudsen diffusivity of species i in a pore and effective Knudsen diffusivity
E = activation energy, J/kmol
k_{s0} = pre-exponential factor of the reaction, $kmol/m^2 \cdot atm \cdot s$
$\underline{\boldsymbol{N}}$ = vector of mass transport fluxes
$\underline{N}_i$ = mass transport flux of species i, $kmol/m^2 \cdot s$
p = total pressure of the mixture, atm
p_i = partial pressure of species i, atm
$\boldsymbol{p}$ = vector of partial pressures
r = pore radius, m
R = ideal gas law constant, J/kmol·K
R_ρ = rate of homogeneous reaction ρ per unit volume, $kmol/m^3 \cdot s$
$R_{v\rho}$ = rate of reaction ρ per unit volume of porous medium, $kmol/m^3 \cdot s$
$R_{s\rho}$ = rate of heterogeneous reaction ρ per unit surface, $kmol/m^2 \cdot s$
S = internal surface area, m^2/m^3
S_i = parameters defined in Eqs. 7a and 7b
t = time, s
T = temperature, K
v_i = molar volume of solid i, m^3/kmol
x_i = mole fraction of species i
$\boldsymbol{x}$ = vector of mole fractions
z = distance variable, m

Greek letters

ϵ = porosity
μ = viscosity of the gaseous mixture, kg/m·s
$\nu_{i\rho}$ = stoichiometric coefficient of species i in reaction ρ
ξ = conversion defined in Eq. 4
Φ^2 = Thiele modulus (see Eq. 24)
ω = dimensionless pre-exponential factor

Subscripts

b = quantities in the gas phase around the preforms
c = quantities at the center of the preforms
i = quantities of species i
s = quantities at the external surface of the preforms
S = quantities of solid product
0 = quantities of unreacted preform or $t = 0$

Superscripts

e = effective quantities
$*$ = reference quantities

Others

MTS = methyltrichlorosilane
CVI = chemical vapor infiltration

Literature Cited

Belitskus, D., "Overview of Ceramic Matrix Composite Fabrication Techniques," *Proc. Conf. on Materials Technol.*, p. 185, M. Genisio, ed., Southern Illinois Univ., Carbondale (1988).

Bird, R. B., W. E. Stewart, and E. N. Lightfoot, *Transport Phenomena*, Wiley, New York (1960).

Besmann, T. M., and M. L. Johnson, "Kinetics of the Low-Pressure Chemical Vapor Deposition of Silicon Carbide," *Proc. Int. Symp. on Ceramic Materials and Composites for Engines*, p. 443, Las Vegas (1988).

Besmann, T. M., B. W. Sheldon, and M. D. Kaster, "Depletion Effects on *SiC* Deposition from MTS," submitted to *J. Amer. Cer. Soc.* (1991).

Brennfleck, K., E. Fitzer, G. Schoch, and M. Dietrich, "CVD of *SiC*-interlayers and Their Interaction with Carbon Fibers and with Multilayered *NbN*-Coatings," *Proc. Int. Conf. on CVD*, M. Robinson et al., eds., p. 649, Electrochem. Soc., Pennington, NJ (1984).

Chung, G. Y., D. Cagliostro, B. J. McCoy, and J. M. Smith, "Process Engineering of Silicon Carbide Matrix Composites," AIChE Meeting, San Francisco (1989).

De Boor, C., *A Practical Guide to Splines*, Springer-Verlag, New York (1978).

Fitzer, E., and R. Gadow, "Fiber-Reinforced Silicon Carbide," *Amer. Ceram. Soc. Bull.*, **65**, 326 (1986).

Gavalas, G. R., "A Random Capillary Model with Application to Char Gasification at Chemically Controlled Rates," *AIChE J.*, **26**, 577 (1980).

Gear, C. W., *Numerical Initial Value Problems in Ordinary Differential Equations*, Prentice Hall, Englewood Cliffs, NJ (1971).

Gupte, S. M., and J. A. Tsamopoulos, "Densification of Porous Materials by Chemical Vapor Infiltration," *J. Electrochem. Soc.*, **136**, 555 (1989).

Langlais, F., R. Naslain, B. Tarride, and C. Prebende, "On the Kinetics of the CVD of Si from SiH_2Cl_2/H_2 and SiC from CH_3Cl_3Si/H_2 in a Vertical Tubular, Hot-Wall Reactor," *J. de Physique*, **50**, C-5(93-103) (1989).

Mason, E. A., and A. P. Malinauskas, *Gas Transport in Porous Media: The Dusty-Gas Model*, Elsevier, New York (1983).

Mason, E. A., A. P. Malinauskas, and R. B. Evans III, "Flow and Diffusion of Gases in Porous Media," *J. Chem. Phys.*, **46**, 3199 (1967).

Middleman, S., "The Interaction of Chemical Kinetics and Diffusion in the Dynamics of Chemical Vapor Infiltration," *J. Mater. Res.*, **4**, 1515 (1989).

Middleman, S., B. Heble, and H. C. T. Cheng, "Improved Uniformity of Ceramic Composites through Control of the Initial Preform Porosity Distribution," *J. Mater. Res.*, **5**, 1544 (1989).

Naslain, R., F. Langlais, and R. Fedou, "The CVI Processing of Ceramic Matrix Composites," *J. de Physique*, **50**, C5-(191-207) (1989).

Papasouliotis, G., and S. V. Sotirchos, "On the Kinetics of SiC Deposition from MTS," ACerS Meeting, Cincinnati (1991).

Rossignol, J. Y., E. Langlais, and R. Naslain, "A Tentative Modellization of Titanium Carbide CVI within the Pore Network of Two-Dimensional Carbon-Carbon Composite Preforms," *Proc. Int. Conf. on CVD*, Robinson et al., eds., p. 596, Electrochem. Soc., Pennington, NJ (1984).

Schlichting, J., "Chemical Vapor Deposition of Silicon Carbide," *Powder Metall. Int.*, **12**, 141, 196 (1980).

Sheldon, B. W., "The Control of Gas-Phase Kinetics to Maximize Densification during Chemical Vapor Infiltration," *J. Mater. Res.*, **5**, 2729 (1990).

Sotirchos, S. V., "On a Class of Random Pore and Grain Models for Gas-Solid Reactions," *Chem. Eng. Sci.*, **42**, 1262 (1987).

Sotirchos, S. V., "Multicomponent Diffusion and Convection in Pore Networks," *AIChE J.*, **35**, 1953 (1989).

Sotirchos, S. V., and M. M. Tomadakis, "Modeling Transport, Reaction, and Structure Evolution during Densification of Cellular or Fibrous Preforms," *Chemical Vapor Deposition of Refractory Metals and Ceramics*, p. 73, T. M. Besmann and B. M. Gallois, eds., MRS, Pittsburgh (1990).

Sotirchos, S. V., and H. C. Yu, "Mathematical Modeling of Gas-Solid Reactions with Solid Product," *Chem. Eng. Sci.*, **40**, 2039 (1985).

Sotirchos, S. V., and H. C. Yu, "Overlapping Grain Models for Gas-Solid Reactions with Solid Product," *I&EC Res.*, **27**, 836 (1988).

Starr, T. L., "Modeling of Forced Flow/Thermal Gradient CVI," *Proc. Int. Conf. Whisk.-Fib.-Tough. Ceram.*, Bradley et al., eds., p. 243, Oak Ridge, TN (1988).

Stinton, D. P., T. M. Besmann, and R. A. Lowden, "Advanced Ceramics by Chemical Vapor Deposition Techniques," *Amer. Ceram. Soc. Bull.*, **67**, 350 (1988).

Stinton, D. P., A. J. Caputo, and R. A. Lowden, "Synthesis of Fiber-Reinforced SiC Composites by Chemical Vapor Infiltration," *Amer. Ceram. Soc. Bull.*, **65**, 347 (1986).

Sugiyama, K., and T. Nakamura, "Pulse CVI of Porous Carbon," *J. Mat. Sci. Lett.*, **6**, 331 (1987).

Sugiyama, K., and E. Yamamoto, "Reinforcement and Antioxidizing of Porous Carbon by Pulse CVI of SiC," *J. Mat. Sci.*, **24**, 3756 (1989).

Tai, N. H., and T. W. Chou, "Analytical Modeling of Chemical Vapor Infiltration in Fabrication of Ceramic Composites," *J. Amer. Ceram. Soc.*, **72**, 414 (1989).

Van Kemenade, A. W. C., and C. F. Stemfoort, "On the Formation of β-SiC from Pyrolysis of CH_3Cl_3Si in H_2," *J. Cryst. Growth*, **12**, 13 (1972).

Whitaker, S., "Diffusion and Dispersion in Porous Media," *AIChE J.*, **13**, 420 (1967).

Zarkanitis, S., E. A. Efthimiadis, and S. V. Sotirchos, "Experimental Evaluation of a Class of Distributed Pore Size Models for Gas-Solid Reactions with Solid Products," *Chem. Eng. Sci.*, **45**, 2761 (1990).

Manuscript received Feb. 12, 1991, and revision received July 3, 1991.